Thermally Driven Morphing and Snap-Through Behavior of Hybrid Laminate Shells

Eric Eckstein, * Alberto Pirrera,†
and Paul M Weaver‡

University of Bristol, Department of Aerospace Engineering. Bristol, BS8 1TR, United Kingdom

Analytical and experimental results are presented regarding the nonlinear temperature-curvature relationship displayed by composite bimorph shells. Snap-through action, driven solely by temperature change, is demonstrated using fiber-metal hybrid laminates. These laminates exploit the high CTE mismatch between composites and metals to yield thermal bimorphs with tailorable properties. In order to predict the potentially nonlinear response of these laminates, an energy-based multistability model is developed and made available online. The model utilizes experimentally measured 1D thermally induced curvatures as input parameters to predict a corresponding shell's 2D flexural behavior. Initial curvature is found to be a critical component in enabling snap-through behavior, especially when partnered with highly orthotropic internal moments. Interestingly, the $[0_n/90_n]$ class of unsymmetric laminates popular in the study of thermally induced bistability are shown to be inherently incapable of displaying thermally driven snap-through behavior, regardless of initial curvature. Modeling results compare well with experiments for a square-planform hybrid laminate. The potential impact of this work is the realization of passively controlled, variable geometry structures which can be triggered to change shape at certain temperatures or within specified temperature ranges. Applications include flow and cooling control of gas turbine engines, spacecraft passive thermal control systems, as well as bimorph-based MEMS systems.

*PhD Student, Advanced Composites Centre for Innovation and Science, AIAA student member

†Lecturer in Composite Structures, Advanced Composites Centre for Innovation and Science, AIAA member

‡Professor in Lightweight Structures, Advanced Composites Centre for Innovation and Science, AIAA member

Nomenclature

$M_{\mathrm{T}i}$	Thermally induced moment components
$\Delta\boldsymbol{\kappa}$	Laminate curvature change vector
κ_i, $\hat{\kappa}_i$, $\kappa_{\mathrm{T}i}$	Current, initial, and thermally induced curvature components
$\boldsymbol{\epsilon}^0$	Midplane strain vector
ϵ_i, $\epsilon_{\mathrm{M}i}$, $\epsilon_{\mathrm{T}i}$	Total, mechanical, and thermally induced strain components
w, $\hat{w}$	Current and initial laminate transverse displacements
$\hat{a}$, $\hat{b}$, $\hat{c}$	Initial curvature shape function coefficients
a, b, c	Current curvature shape function coefficients
c_{ij}, d_{ij} , e_i	Midplane strain function coefficients
Π	Total potential energy
L_x, L_y, h	Laminate planform dimensions and thickness
$\overline{Q}_{ij}$	Lamina transformed constitutive matrix components
$\boldsymbol{A}, \boldsymbol{B}, \boldsymbol{D}$	Laminate stiffness matricies

I. Introduction

A number of applications exist within the aerospace field whereby the desired shape of a variable-geometry structure can be correlated to some environmental temperature. In these cases, thermally driven adaptive structures have the potential to bring their benefits for a low degree of complexity and weight, especially when operating in a passive manner. These structures commonly find use in thermal control systems, from simple household thermostats to spacecraft radiators,[1] however they have also been applied towards aerodynamic control in aero-engine nozzles,[2] turbine tip clearance control systems,[3] and investigated for use in deicing systems.[4] Thermally driven structures can be constructed from materials with good high-temperature properties,[5,6] and because they require no linkages or hinges, they have the potential to bring the benefits of adaptive structures to hostile environments such as gas turbine engine combustors and turbines.[7]

Thermally driven structures are characterized by their ability to exhibit a shape change in response to thermal loading. Several avenues exist for generating the necessary strains, such as shape memory materials,[8] phase-change actuators,[9] and exploitation of thermal expansion.[10] The latter of these is the subject of this study. In particular, we focus on the bimorph concept, whereby two or more constituent materials of mismatched coefficient of thermal expansion (CTE) are joined in a laminate such that each material's thermally induced tensile and compressive stresses act remote from the neutral axis, thus generating bending moments, usually in a biaxial manner.

The use of isotropic materials, however, limits the acceptable range of bimorph geometries available to the designer, a problem which may be overcome through the use of composite materials. Mansfield[11] has shown that because the bending stiffnesses and thermal moments are equal in all directions for an isotropic plate, the energetically preferable direction of bending is determined instead by the plate's geometry and boundary conditions. In the case of free elliptical plates, for example, curvature develops preferentially along the major axis of the plate. Analogous results have been found for rectangular planforms.[12] Bending deformation perpendicular to a laminate's long axis, such as that required for a trailing edge airfoil control surface, would be untenable without the use of directional stiffening mechanisms such as stringers or corrugations. The use of composite materials opens the possibility to create thermal bimorphs which are anisotropic in terms of both stiffness and thermal moments. The direct result is that bimorph actuators may be created which exhibit bending action in a direction determined by material orientations, thus allowing the designer freedom to specify general planform geometries.

Free-standing thermal bimorph beams exhibit approximately linear bending response to temperature change, yet for many applications, the designer may instead want to specify a

highly nonlinear response, such as displacement concentrated within a temperature range, or perhaps even a step-change response. This behavior is currently achievable with isotropic bimorphs using various permutations of either the captive end-constrained beam[13] or shallow dome approaches.[14,15] However, the limited geometrical design space restricts them from general actuation and morphing applications, particularly where the actuator skin is to be employed as an aerodynamic surface. While shape memory alloys may be employed to give nonlinear displacement response to thermal loading, this study seeks to demonstrate that similar behavior can be obtained from bimorphs constructed from more conventional engineering materials, particularly those with favorable structural properties such as high modulus and low density.

Our work seeks to demonstrate that the tailorability of composite materials, combined with the geometrically nonlinear large-displacement response of thin shells, can yield thermal bimorph devices with highly nonlinear displacement response to temperature change. Step-change displacement response, snap-through, and even multistability become possible. No captive end-constraints are necessary, allowing for the sort of cantilevered implementations that would be required for trailing edge aerodynamic surfaces or boom deployment applications. Additionally, exploitation of material anisotropy gives the designer greater geometrical freedom than what is possible with isotropic materials. The use of morphing kinematics may yield variable-geometry systems free of the weight and durability problems of discrete hinges and linkages, especially when applied to hot, oxidizing, or corrosive environments. The ability to tailor snap-through temperatures may prove useful in passive spacecraft deployment applications and aero-propulsion fluidic control, whereby the majority of the actuator stroke can be concentrated within a relatively small temperature range.

The contents of this work are organized as follows: Section II aims to provide the reader with an understanding of the basic principles employed to yield thermally driven morphing and snap-through behavior from composite shells, while Section III discusses the modeling techniques used to predict the behavior of these structures subject to thermal loads. The fabrication of composite shell specimens as well as experimental determination of their thermal response are both detailed in Section IV, while Section V presents results and additional insight into the behavior of thermally loaded composite shell structures.

II. Mechanics

II.A. Achieving Snap-Through Behavior by Exploiting the Geometrically Nonlinear Flexural Response of Thin, Initially Curved Shells

Thin shells with initial curvature display nonlinear bending response when loaded with moments which act to induce curvature perpendicular to the initial curvature direction.[16] Con-

sider the shell shown in Fig. 1, with an applied internal bending moment (perhaps from thermal loading) along the x-direction, $M_{\mathrm{T}x}$. From a beam-mechanics perspective, the effective bending stiffness of the structure as a whole along this direction is a function of not only the laminate's constitutive relations, but also the geometric stiffness granted by the curvature in the y-direction, κ_y. The latter stiffens the plate in the same manner that an extended carpenter's tape measure is stiffened by its transverse curvature. Alternatively, one can view the problem from a shell mechanics perspective, whereby a singly curved surface initially resists development of Gaussian curvature through storage of membrane strain energy. When $M_{\mathrm{T}x}$ exceeds some critical value, it becomes energetically favorable for this thin-walled structure to accommodate load with bending strain energy instead, manifested by curvature generation in the x-direction. As shown in Fig. 1b-c, this increase in κ_x is accompanied by loss of κ_y as required to minimize Gaussian curvature change and its associated membrane strain energy. Returning to the beam perspective, the geometric bending stiffness granted by transverse curvature is lost upon Brazier collapse[17] of the section to a flat strip,[a] allowing the beam to deform in the direction of moment application. This behaviour can be observed by bending a carpenter's tape measure until it snaps into a kinked shape.

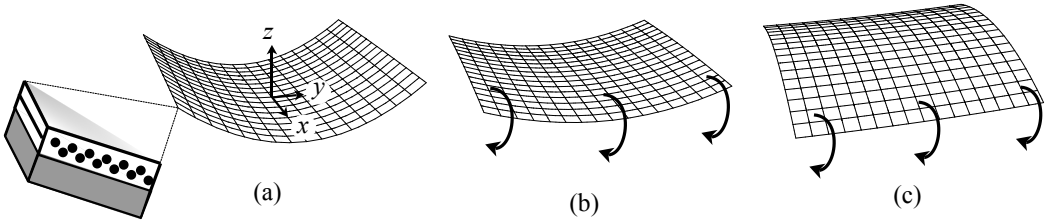

Figure 1. Response of curved shell to applied internal bending moment perpendicular to initial curvature direction. (a) A laminate is constructed with adjacent fiber-composite and metallic layers, with the fibers being oriented perpendicular to the direction of initial curvature. (b) Upon cooling from its stress-free temperature, thermally induced moments develop within the laminate, which are primarily oriented along the fiber direction. (c) When a critical internal moment is reached, the initial curvature is overcome, and the resulting loss of stiffness allows the laminate to snap to a new shape.

The addition of internal bending stresses can allow a curved shell to take on multistable properties,[18] a property which has found application in deployment systems.[19] By controlling the magnitude and direction of internal bending stresses, perhaps via a thermal bimorph arrangement, it is possible to engender a shell structure with highly nonlinear curvature response to temperature change. This behavior may include a rapid (but not necessarily instantaneous) change in shape over a certain temperature range, or in more extreme cases, may include snap-through and multistable behavior.

Figure 2 is a generic example intended to illustrate the role of initial curvature in enabling snap-through behavior triggered by internal moments, such as those arising due to thermal

[a] L.G. Brazier observed that thin-walled beams experience distortions of their cross section under bending loads. Usually, the tendency is for the cross-section to be flattened towards the beam's neutral axis, as would be found by bending a plastic drinking straw until it kinks.

loads. It was created using the multistability model presented in Eckstein et al.[20] for both a square-planform isotropic plate and an cylindrically curved isotropic shell. The internal moments considered are hypothetical, in that their origin is not important, but instead we consider them as generic input loads which my be varied to explore the structure's response. The white regions represent combinations of internal moments which yield only one stable shape, while the colored regions represent combinations which yield bistable behavior. Essentially, the colored regions represent the overlap of each shape's solution space, and thus within this region, there exist two stable shapes. Note that other regions of bistability have been cropped out for clarity, however Fig. 1b from Fernandes et al.[21] gives a complete account of these omitted regions.

Cylindrical initial curvature has the effect of shifting the region of bistability by an amount negatively proportional to, and along the internal moment axis of the initial curvature direction. This shift in response is exemplified by the blue region in Fig. 2, which corresponds to negative cylindrical curvature in the y-direction (as in Fig. 1a). Thus, this region is shifted along the y-axis from the red region. This negatively proportional shift applies so long as the initial curvature is cylindrical. A full explanation of this observation is given in Subsection V.B.

A thermally driven snap-through event occurs when the one laminate shape is driven beyond its stable region as a result of thermally induced internal moments, as graphically illustrated by paths (a) and (b) in Fig. 2. Tracing from the origin, both paths enter the bistable region of the initially cylindrical shell, although no snap-through occurs as of yet because the initial shape remains stable. Upon exit of the bistable region, the initial shape becomes unstable, and the laminate snaps to a cylinder at the points indicated by the circular markers in the same process as described by Fig. 1. Tracing backward towards the origin, snap-through would instead occur at the square markers, as these represent the points where the second shape ceases to be stable, resulting in a snap-through transition back to the initial shape.

The conditions required for snap-through behavior are now discussed. In the case of a thermally driven bimorph, the internal moments $M_{\mathrm{T}x}$ and $M_{\mathrm{T}y}$ are both proportional to temperature, barring slight variations due to temperature-dependent material properties. Paths (a), (b), and (c) in Fig. 2 demonstrate this proportionality, in that they are straight lines emanating from the origin. Under these circumstances, we can observe that for an initially flat plate, any straight path drawn from the origin may enter, but never exit the red region. That is to say that snap-through is not possible with initially flat plates subject to proportional moments, such as those driven by temperature change. Path (c) represents the special case of curvature bifurcation upon entering the bistable region as described by Hyer,[22] however this behavior is not to be mistaken for a snap-through process as the curvatures

are still continuous with respect to temperature. For proportional moments such as those generated by thermal bimorphs, initial curvature is a necessary ingredient for snap-through behavior, as it allows paths such as (a) and (b) to traverse and exit the blue bistability region. We can generalize this finding by stating that any point along the boundary of a bistability region is eligible for snap-through driven by proportional moments, so long as a line drawn between this point and the origin also intercepts another boundary of the same region.

In addition, we can also conclude from Fig. 2 that the moments generated cannot be equal and opposite for snap-through behavior. This conclusion is exemplified by path (c), which even in the case of initial curvature, would only enter a bistable region, but never achieve the necessary exit required for snap-through. This observation implies that the unsymmetric $[0_n/90_n]$ class of laminates popular in the study of bistability are inherently incapable of displaying thermally driven snap-through behavior, regardless of the laminate's initial curvature.[b] In order to achieve snap-through as demonstrated by paths (a) and (b), the magnitude of $M_{\mathrm{T}x}$ and $M_{\mathrm{T}y}$ must be made sufficiently unequal, specifically $M_{\mathrm{T}x}$ must have greater magnitude than $M_{\mathrm{T}y}$ in the case of the initial curvature direction illustrated in Fig. 1. Such unequal moments can be achieved using a highly biased layup such as $[0_1/90_7]$, however in practice, such layups showed troublesome matrix cracking issues in the course of the authors' efforts. A more successful solution to the challenge of generating unequal moments is described in Subsection II.B.

One may also observe that with sufficient initial curvature, equal and same-sign moments can also yield snap-through behavior. Although such a path is not shown on Fig. 2, it can be visualized by mirroring path (c) about the x-axis. This path would intersect the bistability region of an initially cylindrical shell, as long as the initial curvature of that shell was sufficient that its region of bistability intersected with the mirror of path (c). It is also worth noting that if one is not constrained by the proportional internal moments inherent in thermal bimorphs, it would be possible to achieve a moment path which need not be a straight line emanating from the origin. Such a path could criss-cross the bistable region according to the designer's wishes. In other words, the ability to actuate $M_{\mathrm{T}x}$independently from $M_{\mathrm{T}y}$, perhaps via piezoelectric actuators, would allow snap-through to be achieved in a laminate possessing any degree of initial curvature. This consideration is beyond the scope of the present work, however Fernandes et al.[21] have studied this concept in-depth.

[b]We note that although $[0_n/90_n]$ laminates are not isotropic, their stability map is qualitatively similar to Fig. 2 on account of their equal bending stiffness and thermal moment magnitudes in the x and y directions.

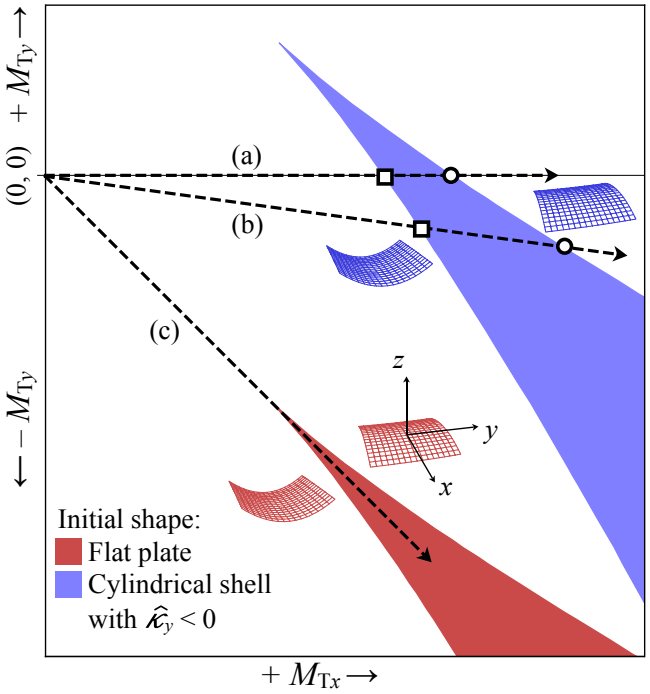

Figure 2. Stability map showing combinations of hypothetical internal bending moments M_{Tx} and M_{Ty} which yield bistable behavior for an isotropic square-planform flat plate and shell with initial curvature $\hat{\kappa}_y$, as illustrated by Fig. 1a, Bistable regions are denoted by color shading. The illustrated shell curvatures adjacent to each region represent the two stable shapes attained within the region, as well as the monostable shapes which exist outside the respective region boundaries. Dashed lines indicate internal moment paths for three example cases: (a) Unidirectional moment. (b) Proportional moments of unequal and opposite sign, which represent the present hybrid laminates. (c) Proportional moments of equal magnitude and opposite sign, which represent the $[0_n/90_n]$ class of bistable laminates. Circular markers denote snap-through points for increasing moments, while square markers denote the same for decreasing moments.

II.B. Generation of Internal Moments using Composite Bimorphs

The basic mechanics of how composite bimorphs create internal bending moments are similar to that of isotropic bimorphs, however whilst isotropic bimorphs exert omnidirectional moments, those from a composite bimorph can be highly directional on account of the composite layer's anisotropic elastic and thermal expansion properties. This anisotropy not only brings the tailorability advantages discussed in Section I, but as mentioned in Subsection II.A, is essential in enabling snap-through behavior.

The current work focuses on the composite bimorph shown in Fig. 3. This bimorph utilizes a low-expansion unidirectional composite layer bonded to a high-expansion isotropic metallic layer, inspired by the work of Asanuma et al.[23] Thermal moments are primarily generated along the fiber direction, about which the laminate's flexural stiffness and CTE mismatch is maximized. Secondary thermal moments along the perpendicular direction are present if the fibrous layer's CTE is mismatched to the metallic layer. In this work, we utilize Hexcel AS7/M21 unidirectional prepreg as the low-expansion layer, and 5251 aluminum alloy as the high-expansion layer, for which material properties are given in Table 1.

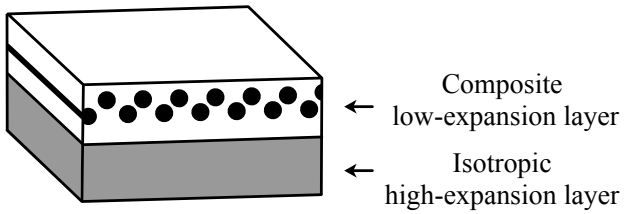

Figure 3. Diagram showing the cross-section of the bimorph laminate under investigation, which is embodied in this work as a CFRP-metal hybrid laminate.

Strictly speaking, it is not necessary to always specify the composite layer as the low-expansion element, however given that thermoelastic anisotropy and high modulus are both desired, the choice of materials narrows to fibrous composites based upon engineering fibers such as carbon, glass, and silicon carbide. These materials all have relatively low fiber-direction CTEs, thus encouraging their use in the low-expansion element. Likewise, the isotropic layer need not be the high-expansion element, however certain structural metals such as aluminum and austenitic stainless steel alloys are excellent candidates on account of their high modulus and thermal expansion coefficients. It should also be noted that the desired anisotropy can still be achieved when only one of the two layers possesses anisotropic thermoelastic properties.

II.B.1. Alternatives to Unidirectional Fiber Orientations

Although we only consider unidirectional layups in our analysis and experiment, we note that potentially advantageous laminate properties may be achieved using shallow angle-ply

layups having orientation angles generally smaller than $\pm 30^\circ$ about the x-axis. Halpin and Pagano[24] have shown that for composites in which the fiber and matrix CTEs are highly mismatched (e.g. carbon-epoxy), shallow angle ply layups can yield a laminate with a lower CTE along one axis than its constituent lamina possess along any axis. This feature can be explained by the fact that angle-ply laminates can have a very high Poisson's ratio, and thus if the angle ply laminate has a high CTE in the y-direction, Poisson effects will drive an opposite strain in the x-direction, which depresses the CTE along that direction. The utility of this result is that shallow angle-ply laminates can have a greater CTE mismatch with the high-expansion layer in a composite bimorph than that possible using a unidirectional layup, thus yielding greater curvature change for a given temperature change.

Halpin and Pagano also noted that the y-direction CTE of angle-ply layups can also be tailored based on fiber orientation angle, thus it is possible to create an angle-ply layup whose y-direction CTE is matched to the high-expansion layer's CTE. As a result, it is likely feasible to create composite bimorphs which generate completely unidirectional thermal moments along the x-direction, i.e., there would be no thermal moments in the y-direction. This feature could be useful if the designer wished to avoid generation of transverse curvature, or to create a composite bimorph with completely unidirectional actuation moments and displacements, regardless of planform shape. Serendipitously, the orientation angles which match a CFRP angle ply laminate's CTE with aluminum alloy along one axis happen to fall within the range of orientation angles which yield negative CTEs along the perpendicular axis. For example, a simple classical lamination theory analysis of typical intermediate modulus carbon-epoxy prepreg composite predicts that a $[+23^\circ/-23^\circ]_n$ laminate would have a y-direction CTE matched to the $23 \times 10^{-6}/^\circ\text{C}$ of most aluminum alloys at room temperature. The composite layer's x-direction CTE would be approximately $-2.9 \times 10^{-6}/^\circ\text{C}$, thus increasing its CTE mismatch with the aluminum layer by roughly 12% over what would be achieved with a 0° unidirectional layup. As a concluding point, we hope such considerations may prompt follow up work in this area.

III. Modeling Methodology

Researchers in the field of multistable structures have produced a host of analytical models aimed at predicting the large-displacement response of initially curved shells to internal moments,[25–27] and thus this type of model forms the basis of our analysis. In particular, we build upon prior work[20] to model the response of an initially curved composite thermal bimorph. In summary, this model finds the stable shapes of thin anisotropic laminates with free-free boundary conditions using a Raleigh-Ritz energy minimization scheme. Utilizing modified von Kármán plate kinematics, it accounts for initial curvature and temperature-dependent

material properties. The model utilizes second order polynomial shape and strain functions to approximate the laminate's transverse displacement and membrane strains, respectively. These relatively low-order shape and strain functions give rapid solutions, however they have poor accuracy relative to higher order methods in predicting the laminate's curvatures near snap-through temperatures. The second order nature of the transverse displacement shape functions allows them to capture constant curvatures only, and thus they cannot resolve variations of curvature near free edge boundaries. Nonetheless, these functions remain suitable for capturing the laminate's overall curvature response, which is the main focus of this study.

The modelling novelty can be summarized as follows: In the present modelling technique, thermally induced curvatures are first measured from representative strips of a laminate across a range of temperatures. The model then uses these measured 1D curvatures to calculate the thermally induced 2D curvatures of a shell constructed from the same layup. The main result is that the model no longer requires thermal expansion coefficient material data, nor does it need the laminate's stress-free temperature. In addition, other strain-inducing effects such as resin cure shrinkage are automatically accounted for with this approach.

III.A. Description of Thermal Curvature

Classically, the loads on the structure would be determined via computation of thermal stresses, which would then be integrated across the laminate's thickness to find internal moments and stress resultants. The thermal stresses themselves would be computed from the prescribed temperature change and known thermoelastic material data, namely thermal expansion coefficients and moduli. The shortcoming of this approach towards calculating thermal loads is that the complete stress state must be known at some reference temperature. Previous workers have generally used the cure temperature as that reference, for which a zero-stress state was assumed.[22,26,28] While this approach simplifies calculations and provides convenient comparisons with finite element models, it ignores the presence of non-thermoelastic strains such as plastic deformation, resin shrinkage, or tool-part interactions. Our recent work with hybrid fiber-metal laminates, as well as congruent research,[29] has revealed that non-thermoelastic strains generally cannot be neglected, as they can significantly affect predicted curvatures. Because these strains are highly layup and process-dependent,[30] reliably calculating them *a priori* for general cases is presently regarded as impractical.

Instead, we propose a technique in which the components of the thermally induced curvature vector $\boldsymbol{\kappa}_{\mathrm{T}}$ are each experimentally measured at all temperatures of interest, and the resulting values are utilized directly as loading inputs into our model's total potential energy expression. In the scope of this work, these thermal curvatures are due to thermal expansion strain, however in general cases they may arise from other actuation strain sources such

as hydroscopic or shape-memory-induced strain.[c] Thermal curvatures are defined as the curvature change the laminate would achieve in an unrestrained state, i.e., if it were freed from the geometrically nonlinear kinematics which otherwise restrain its deformation. In this state, curvatures are decoupled from membrane strains, and thus any thermally induced internal bending moment translates directly and proportionally to thermal curvature. For this reason, thermal curvatures are in fact coincident to the those that would be predicted by linear classical laminated plate theory. Thermal curvature along a given direction may be measured by fabricating a long, narrow (i.e. beam-like) strip of the laminate under investigation, such that the stiffening effects of transverse curvature[16] are negligible. As long as no mechanical loads are applied, the curvature observed in the resulting strip is the thermal curvature of the laminate along the strip's lengthwise direction. This approach of using experimentally measured thermal curvatures as loading inputs effectively amounts to replacing the conventional uniaxial measurement of CTEs with a flexural measurement of CTE mismatch. Besides automatically accounting for non-thermoelastic strains, this approach also avoids the need for the specialized instrumentation required for uniaxial CTE measurement, as thermal curvature may instead be quantified with any number of flexural displacement-measuring techniques such as laser metrology or even simple dial gauges. Our use of thermal curvature is not new, particularly in the field of multistability where it has been referred to generically as *inelastic curvature* or *relaxed curvature*. In particular, we adopt the original symbology of Mansfield while incorporating prior techniques for computing total potential energy in terms of thermal curvatures.[14,31,32]

III.B. Model Development

A schematic drawing of the Cartesian modeling space is given in Fig. 4. Although the structure has the geometry of a shell, it is modeled mathematically as an initially curved plate using an approach similar to that employed by Mansfield for bending analysis of initially curved strips.[33] Thus, the presently analyzed structure is technically a curved plate for the sake of mathematical consistency, though it still displays shell-like behavior. Note that side lengths are given as arc lengths along the edges. This ensures that total potential energy is being integrated across the actual area of the laminate, as opposed to just the area projected onto the x-y plane.

In this work, we assume the laminate to have free edges, while being constrained only at the origin. This scenario allows fairly generic results to be presented, however it ignores the practical implications of attachment and integration into a broader structure. Several workers

[c]The model makes no distinction regarding the type or source of expansion strain. It would be perfectly admissible to measure the components of $\boldsymbol{\kappa}_{\mathrm{T}}$ against any number of environmental variables, e.g. voltage in piezoelectric laminates, or moisture content of biological materials.

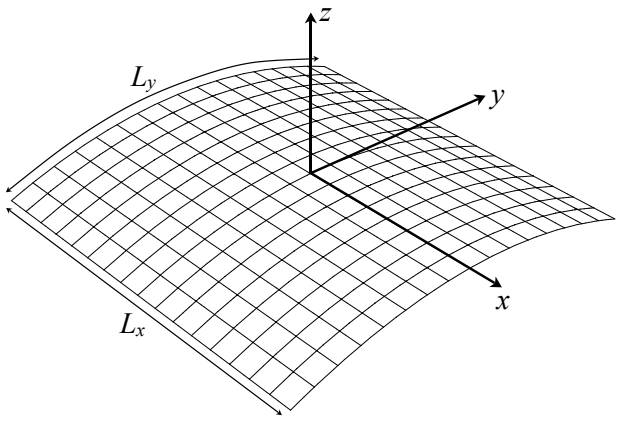

Figure 4. The laminate under investigation is rectangular in planform shape, with Cartesian coordinates centered upon it. Initial curvature and twist is permissible in all directions, however in this illustration, only curvature along the y-direction is shown.

have addressed this issue by various means, including usage of a compliant interface region,[34] or specifying shape functions which directly enforce a clamped boundary condition.[35]

An overview of the model's development is now discussed. The initial (i.e. unstressed) transverse displacement of the plate from the x-y plane, $\hat{w}$, is approximated by the second-order polynomial shape function

$$\hat{w} = \frac{1}{2}\left(\hat{a}x^2 + \hat{b}y^2 + \hat{c}xy\right), \tag{1}$$

where $\hat{a}$, $\hat{b}$, and $\hat{c}$ are shape function coefficients related to the initial curvatures of the plate. Similarly, the current displacement of the plate, w, is written as[28]

$$w = \frac{1}{2}\left(ax^2 + by^2 + cxy\right), \tag{2}$$

where a, b, and c are related to the current x, y, and twist curvatures respectively. Note that w represents the plate's total displacement from the x-y plane, and not the displacement from the initially unstressed state. As we are concerned with obtaining an expression for total potential energy in terms of curvatures and midplane strains, we define a vector that represents the curvature quantities that result in the generation of strain energy. Specifically, this is the difference between the initial and current plate curvatures, which are defined from the second derivative of transverse displacement as

$$\Delta\boldsymbol{\kappa} = \begin{Bmatrix} \kappa_x - \hat{\kappa}_x \\ \kappa_y - \hat{\kappa}_y \\ \kappa_{xy} - \hat{\kappa}_{xy} \end{Bmatrix} = \begin{Bmatrix} -\left(\frac{\partial^2 w}{\partial x^2} - \frac{\partial^2 \hat{w}}{\partial x^2}\right) \\ -\left(\frac{\partial^2 w}{\partial y^2} - \frac{\partial^2 \hat{w}}{\partial y^2}\right) \\ -2\left(\frac{\partial^2 w}{\partial x\,\partial y} - \frac{\partial^2 \hat{w}}{\partial x\,\partial y}\right) \end{Bmatrix} = \begin{Bmatrix} \hat{a} - a \\ \hat{b} - b \\ \hat{c} - c \end{Bmatrix}. \tag{3}$$

As before, the hat symbol denotes quantities measured in the initial state. Note that twist curvature κ_{xy} is defined using the engineering convention to maintain consistency with classical lamination theory. Midplane strain functions are specified on a second order basis per the form developed by Dano and Hyer.[28] :

$$\epsilon_x^0 = c_{00} + c_{20}x^2 + c_{02}y^2 + c_{11}xy, \tag{4}$$

$$\epsilon_y^0 = d_{00} + d_{20}x^2 + d_{02}y^2 + d_{11}xy, \tag{5}$$

where the c_{ij} and d_{ij} terms are strain function coefficients. Midplane strains must satisfy compatibility of a curved surface, thus the final component γ_{xy}^0 cannot be defined independently of ϵ_x^0 and ϵ_y^0. This compatibility relation is adapted from Calladine[36] as

$$\kappa_x\kappa_y - \frac{\kappa_{xy}^2}{4} - \left(\hat{\kappa}_x\hat{\kappa}_y - \frac{\hat{\kappa}_{xy}^2}{4}\right) = -\frac{\partial^2\epsilon_x^0}{\partial y^2} - \frac{\partial^2\epsilon_y^0}{\partial x^2} + \frac{\partial^2\gamma_{xy}^0}{\partial y\partial x}. \tag{6}$$

Note that by computing curvature as the second derivative of transverse displacement in Cartesian coordinates (i.e. Eq. (3)), Eq. (6) becomes an equivalent statement to von Kármán's plate kinematics.[d] We obtain a strain function approximating γ_{xy}^0 by substituting Eqs. (3-5) into Eq. (6). Solving the resulting expression for γ_{xy}^0 by integration yields

$$\gamma_{xy}^0 = e_1 + e_3x^2 + e_5y^2 + \left(ab - \frac{c^2}{4} - \left(\hat{a}\hat{b} - \frac{\hat{c}^2}{4}\right) + 2c_{02} + 2d_{20}\right)xy. \tag{7}$$

The e_i terms are constants of integration which take on the role strain function coefficients similar to the c_{ij} and d_{ij} terms in Eqs. (4-5). Nonlinearity is introduced to the problem via Eq. (7). The presence of the midplane strain coefficients c_{02} and d_{20} in the same term as the curvature coefficients is the means by which the problem's nonlinearity is propagated to ϵ_x^0 and ϵ_y^0, as the those two coefficients are shared between strain functions. The reader should note that we could have just as well specified strain functions for, say, ϵ_x^0 and γ_{xy}^0, and then used Eq. (6) to find ϵ_y^0 just as we previously did for γ_{xy}^0. Thus, there is no special significance to the fact that Eq. (7) has a different appearance than Eqs. (4-5).

The total potential energy of a laminate not subject to external forces, whilst neglecting transverse shear and through-thickness stress, is given, for example, by Reddy[37] as

$$\Pi = \int_{\frac{-L_x}{2}}^{\frac{L_x}{2}}\int_{\frac{-L_y}{2}}^{\frac{L_y}{2}}\int_{\frac{-h}{2}}^{\frac{h}{2}} \frac{1}{2}\sigma_i\epsilon_{\mathrm{M}i}\,dz\,dy\,dx, \tag{8}$$

[d]This can be verified by substituting von Kármán's midplane strain equations, modified to account for initial curvature, (e.g. $\epsilon_x^0 = \frac{\partial u}{\partial x} + \frac{1}{2}\left((\partial w/\partial x)^2 - (\partial\hat{w}/\partial x)^2\right)$) into Eq. (6)

where σ_i are the in-plane mechanical stress components, $\epsilon_{\mathrm{M}i}$ are the in-plane mechanical strain components, and h is the thickness of the laminate. As per classical lamination theory convention, $i = x,\ y,\ xy$, with summation of repeated indices implied as per Einstein notation. Mechanical strains are those which are coupled to mechanical stresses via constitutive relations, and sum with thermal strains $\epsilon_{\mathrm{T}i}$ to give total strains ϵ_i as

$$\epsilon_i = \epsilon_{\mathrm{M}i} + \epsilon_{\mathrm{T}i}. \tag{9}$$

Our task now is to write Eq. (8) in terms of total and thermal strains. First, we substitute the lamina constitutive relations $\sigma_i = \overline{Q}_{ij}\epsilon_{\mathrm{M}j}$ into Eq. **(8)**, yielding

$$\Pi = \int_{\frac{-L_x}{2}}^{\frac{L_x}{2}} \int_{\frac{-L_y}{2}}^{\frac{L_y}{2}} \int_{\frac{-h}{2}}^{\frac{h}{2}} \frac{1}{2} \epsilon_{\mathrm{M}i} \overline{Q}_{ij} \epsilon_{\mathrm{M}j}\, dz\, dy\, dx. \tag{10}$$

Next, we solve Eq. (9) for $\epsilon_{\mathrm{M}i}$ and substitute the result into Eq. (10) to give

$$\Pi = \int_{\frac{-L_x}{2}}^{\frac{L_x}{2}} \int_{\frac{-L_y}{2}}^{\frac{L_y}{2}} \int_{\frac{-h}{2}}^{\frac{h}{2}} \frac{1}{2} \left(\epsilon_i - \epsilon_{\mathrm{T}i}\right) \overline{Q}_{ij} \left(\epsilon_j - \epsilon_{\mathrm{T}j}\right)\, dz\, dy\, dx. \tag{11}$$

Assuming transverse shear effects are negligible, our total and thermal strains are decomposed into midplane extension and curvature components as

$$\epsilon_i - \epsilon_{\mathrm{T}i} = \left(\epsilon_i^0 - \epsilon_{\mathrm{T}i}^0\right) + z\left(\Delta\kappa_i - \kappa_{\mathrm{T}i}\right), \tag{12}$$

where ϵ_i^0 and $\epsilon_{\mathrm{T}i}^0$ represent midplane total and thermal strains, respectively; while $\Delta\kappa_i$ and $\kappa_{\mathrm{T}i}$ are the curvature changes from the initial state and thermal curvatures, respectively. Next, Eq. (12) is substituted into Eq. (11), and the integral is evaluated through the thickness. The evaluation of this integral yields terms identical to the classical definitions of the $\boldsymbol{A}$, $\boldsymbol{B}$, and $\boldsymbol{D}$ laminate constants,[37] and thus they are substituted into the result to give

$$\Pi = \int_{\frac{-L_x}{2}}^{\frac{L_x}{2}} \int_{\frac{-L_y}{2}}^{\frac{L_y}{2}} \left(\frac{1}{2} \begin{Bmatrix} \boldsymbol{\epsilon}^0 - \boldsymbol{\epsilon}_{\mathrm{T}}^0 \\ \Delta\boldsymbol{\kappa} - \boldsymbol{\kappa}_{\mathrm{T}} \end{Bmatrix}^{\top} \begin{bmatrix} \boldsymbol{A} & \boldsymbol{B} \\ \boldsymbol{B} & \boldsymbol{D} \end{bmatrix} \begin{Bmatrix} \boldsymbol{\epsilon}^0 - \boldsymbol{\epsilon}_{\mathrm{T}}^0 \\ \Delta\boldsymbol{\kappa} - \boldsymbol{\kappa}_{\mathrm{T}} \end{Bmatrix} \right) dy\, dx. \tag{13}$$

Note that the tensorial notation has been dropped for vector representation, while the superscripted symbol $\top$ denotes transpose.

Further simplifications are possible if we restrict ourselves to uniform thermal strain in the x-y directions. Fernandes et al.[21] have shown that for plates and shells with free boundary conditions, midplane strains due to in-plane material growth only contribute to the total potential energy of the plate when they vary at equal to or greater than second order

with respect to the spatial dimensions, on account of the second order differential nature of Gauss' *Theorema Egregium*. In other words, the growth due to thermal midplane strain is not resisted mechanically in any manner when thermal midplane strains vary spatially at less than second order, thus there can be no storage of strain energy on account of it. The direct result is that if we assume the distribution of thermal strain is invariant across the planform of the laminate, we may neglect the thermal midplane strain terms $\boldsymbol{\epsilon}^0_{\mathrm{T}}$. Nonetheless, we must still retain the total midplane strain terms in order to account for membrane strain energy arising due to change in the laminate's Gaussian curvature. The final form of our total potential energy expression is thus:

$$\Pi = \int_{\frac{-L_x}{2}}^{\frac{L_x}{2}} \int_{\frac{-L_y}{2}}^{\frac{L_y}{2}} \left(\frac{1}{2} \left\{ \begin{array}{c} \boldsymbol{\epsilon}^0 \\ \Delta\boldsymbol{\kappa} - \boldsymbol{\kappa}_{\mathrm{T}} \end{array} \right\}^{\top} \begin{bmatrix} \boldsymbol{A} & \boldsymbol{B} \\ \boldsymbol{B} & \boldsymbol{D} \end{bmatrix} \left\{ \begin{array}{c} \boldsymbol{\epsilon}^0 \\ \Delta\boldsymbol{\kappa} - \boldsymbol{\kappa}_{\mathrm{T}} \end{array} \right\} \right) dy\, dx. \tag{14}$$

The loading terms contained within $\boldsymbol{\kappa}_{\mathrm{T}}$ are sourced by experimental measurement in this work, however they may be calculated from material data using classical lamination theory if desired. The procedure is outlined by Collier,[38] whereby the author also describes how thermal curvatures may be modelled in an FE implementation.

At this point, the shape and strain functions from Eqs. (1-7) are substituted into the $\Delta\boldsymbol{\kappa}$ and $\boldsymbol{\epsilon}^0$ terms within Eq. (14). The integral is evaluated, yielding a scalar expression for total potential energy in terms of the shape and strain function coefficients, constitutive constants, and thermal curvatures. Equilibrium shapes are found by computing variations of Π with respect to each shape function coefficient, and setting all variations to zero as follows:

$$\left\{ \frac{\delta\Pi}{\delta a}, \frac{\delta\Pi}{\delta b}, \frac{\delta\Pi}{\delta c}, \frac{\delta\Pi}{\delta c_{00}}, \frac{\delta\Pi}{\delta c_{20}}, \frac{\delta\Pi}{\delta c_{02}}, \frac{\delta\Pi}{\delta c_{11}}, \frac{\delta\Pi}{\delta d_{00}}, \frac{\delta\Pi}{\delta d_{20}}, \frac{\delta\Pi}{\delta d_{02}}, \frac{\delta\Pi}{\delta d_{11}}, \frac{\delta\Pi}{\delta e_1}, \frac{\delta\Pi}{\delta e_3}, \frac{\delta\Pi}{\delta e_5} \right\} = 0. \tag{15}$$

Energy equilibria are obtained when values of the shape function coefficients are found which simultaneously satisfy all of the equalities in Eq. (15). In practice, this system can partially be solved symbolically to give solutions for c_{ij}, d_{ij} , and e_i in terms of only a, b, and c. This result is substituted into the remaining system $\left\{ \frac{\delta\Pi}{\delta a}, \frac{\delta\Pi}{\delta b}, \frac{\delta\Pi}{\delta c} \right\} = 0$, which is subsequently solved numerically using a Newton-type scheme. We note that Betts et al.[39] and Hernandez et al.[40] have reported success in obtaining closed form solutions for specific geometry and constitutive properties. Second variations are used to determine the stability of each of the equilibria as per the procedure described in Hyer's seminal work.[22] The process is then repeated for all thermal curvatures of interest.

This model was implemented using Wolfram Mathematica 10, and is available online via the supplemental data attachment to this article.

IV. Experimental Methodology

IV.A. Fabrication of Hybrid Laminate Shell and Strip Specimens

This section concerns the construction of fiber-metal hybrid laminates, as depicted in Fig. 3. Three laminates were constructed according to the parameters given in Table 2. All three laminates were fabricated from a layer of 5251 aluminum, bonded to a layer of Hexcel AS7/M21 unidirectional prepreg carbon composite, and autoclave cured on a cylindrically curved aluminium tool at 180°C. The aluminum layer acts as the high-expansion element, and is complemented by the high-stiffness, low expansion composite layer to yield predominately unidirectional thermal moment upon thermal loading. Prior to curing, the 5251Al layer was prepared for bonding by scuffing with P200 silicon carbide sandpaper,[e] and roll-formed to match the tool curvature. The epoxy contained within the prepreg material was used as the bonding agent, and thus the curing of the composite layer and bonding to the aluminum layer was carried out simultaneously during autoclave processing. Two of the laminates were cured on a flat tool, and strips of 230 mm length and widths between 10 mm and 50 mm were cut from them oriented parallel to the fibers for one plate, and perpendicular for the other. Observation of the room temperature curvature of these strips showed that the stiffening effects of transverse curvature were insignificant for strips widths of less than 30 mm, and thus we concluded that strips of 20 mm width would yield accurate measurements of $\kappa_{\mathrm{T}x}$ and $\kappa_{\mathrm{T}y}$. Due to the nature of the laminate, no twist curvature $\kappa_{\mathrm{T}xy}$ was anticipated. This assertion is supported by results from the testing described in the following section.

Temperature-dependent material data for Hexcel AS7/M21 UD prepreg was obtained by experiment as described in Eckstein et al.,[20] and is copied in Table 1 for convenience. Material data for 5251 aluminum alloy was sourced from the ESDU Metallic Materials Data Handbook,[41] and is also shown in Table 1. Where data at intermediate temperature values was unavailable, data from similar alloys was utilized to aid interpolation.

IV.B. Measurement of Thermal Curvatures and Snap-Through Behavior of Hybrid Laminate Shells

Shell and strip displacements were measured by digital image correlation (DIC), an optical 3D displacement measurement technique. The test articles were mounted on a steel rig using

[e]Sandblasting was also found to be an effective method of surface preparation from a bond strength standpoint, however this process creates residual compressive stresses upon the surface of the aluminum sheet similar to the mechanics of shot-peening. These stresses are eccentric to the sheet's neutral axis, and their resulting moments induce curvatures in the sheet. This can be mitigated by sandblasting both sides of the sheet to an equal degree, or one can simply accept the residual stresses as they are. As long as the same preparation method is used to fabricate the strips used to measure $\kappa_{\mathrm{T}x}$ and $\kappa_{\mathrm{T}y}$, the curvature induced by these residual stresses will be fully accounted for within the analytical model.

Table 1. Thermoelastic material data for AS7/M21 UD composite and 5251 aluminium alloy. Although the present model does not require thermal expansion material data, it is provided here nonetheless to aid with the reader's understanding of the results. Thermal expansion coefficients use a reference temperature of 20°C.

	Hexcel AS7/M21 UD Prepreg						Al 5251		
Temp. [°C]	E_1 [GPa]	E_2 [GPa]	G_{12} [GPa]	ν_{12} [-]	α_1 $[\frac{10^{-6}}{°C}]$	α_2 $[\frac{10^{-6}}{°C}]$	E [GPa]	ν [-]	α $[\frac{10^{-6}}{°C}]$
30	129.55	8.85	5.28	0.33	-2.3	23.4	72.0	0.33	23.0
60	127.99	8.42	4.88	0.33	-2.1	27.8	71.3	0.33	23.0
90	127.47	7.92	4.65	0.33	-1.5	28.6	70.6	0.33	23.0
120	127.18	7.57	4.50	0.33	-0.5	30.0	69.8	0.33	23.2
150	126.11	7.18	4.26	0.33	1.7	32.1	68.4	0.33	23.4
170	125.58	6.76	4.01	0.33	2.6	33.5	67.7	0.33	23.6
180	125.31	6.48	3.77	0.33	2.3	33.5	67.0	0.33	23.6

Table 2. Test article manufacturing parameters for hybrid fiber-metal laminates.

	0° strip cut from 230×230 mm plate for measurement of $\kappa_{\mathrm{T}x}$	90° strip cut from 230×230 mm plate for measurement of $\kappa_{\mathrm{T}y}$	Curved shell for evaluation of thermally driven snap-through behavior
Layup	$[\mathrm{Al}_1/0_4^\circ]$	$[\mathrm{Al}_1/90_4^\circ]$	$[\mathrm{Al}_1/0_4^\circ]$
5251 Al sheet thickness [mm]	1.20	1.20	1.20
AS7/M21 ply thickness [mm]	0.286	0.286	0.286
Side lengths [mm]	230 x 20	230 x 20	230 x 230
Tool curvature $\hat{\kappa}_x[\mathrm{mm}^{-1}]$	0	0	0
Tool curvature $\hat{\kappa}_y[\mathrm{mm}^{-1}]$	0	0	$-1/400$

a single M6 fastener secured to a post, and placed in an oven as shown below in Fig. 5. Thermocouples were adhered to the composite layer with the aid of conductive paste both near and afar from the mounting post. Their readings were compared to ensure that the thermal lag induced by heat conduction to the test rig was minimal. In the course of testing, the thermocouple readings diverged by no more than 4°C. Temperature was ramped from 20°C-180°C at a rate of 2°C/min, then back down to 20°C at an equal rate.

Each DIC frame captures the displacements of approximately 20,000 points across the area of the shell. Curvatures κ_x , κ_y, and κ_{xy} are determined by fitting the measured displacements to a surface of the form $w = \frac{1}{2}\left(ax^2 + by^2 + cxy\right)$. The fitting coefficients a, b, and c yield the curvatures via the following relations

$$\left\{ \begin{array}{c} \kappa_x \\ \kappa_y \\ \kappa_{xy} \end{array} \right\} = \left\{ \begin{array}{c} -\frac{\partial^2 w}{\partial x^2} \\ -\frac{\partial^2 w}{\partial y^2} \\ -2\frac{\partial^2 w}{\partial x\, \partial y} \end{array} \right\} = \left\{ \begin{array}{c} -a \\ -b \\ -c \end{array} \right\}. \tag{16}$$

An identical temperature profile and curvature measurement procedure is utilized for measuring the thermal curvatures of the strip specimens.

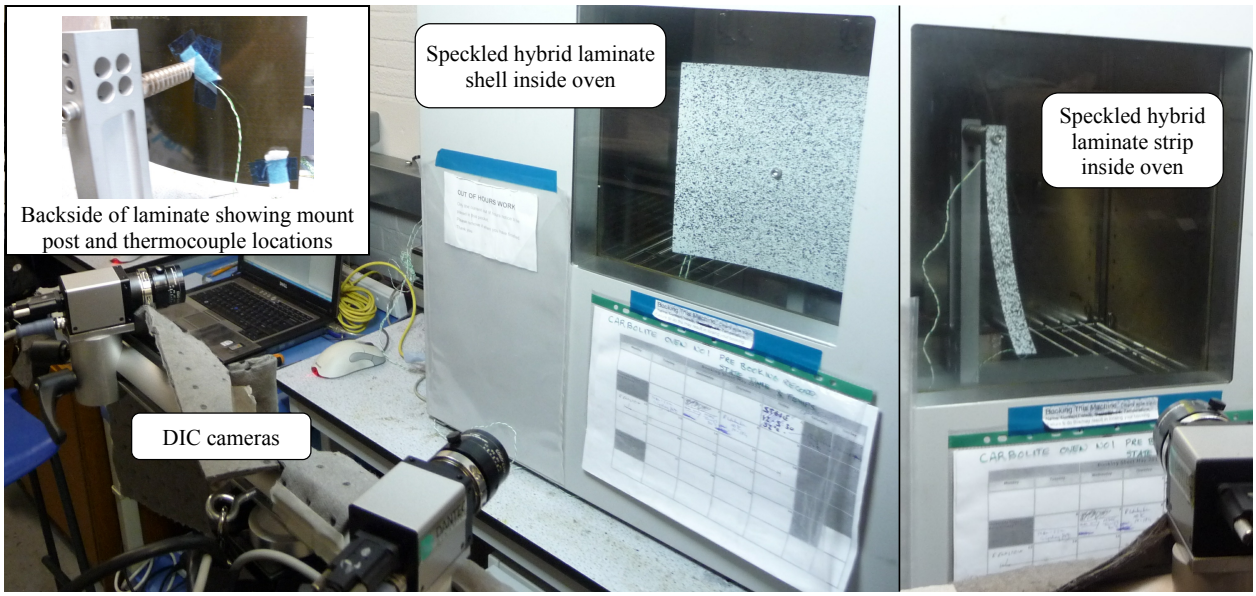

Figure 5. Hybrid laminate test setup, showing speckled shell (left) and strip (right) test articles mounted inside oven.

V. Results and Discussion

V.A. Experimental Measurements of Thermal Curvature

The thermal curvatures measured from the strip specimens specified in Table 2 are plotted in Fig. 6. This figure is best viewed from right to left, on account of the fact that thermal strains increase as temperature decreases. This measurement of non-zero thermal curvature at cure temperature (180°C) indicates the presence of non-thermoelastic strains. As mentioned in Subsection III.A, these strains are likely due to resin shrinkage and/or tool-part interactions. Throughout the measured temperature range, κ_{Tx} varies linearly with temperature, barring minor perturbations. This trend falls in line with expectations, as both the composite and metallic layers have nearly constant CTE values with respect to temperature, in the direction parallel to the fibers. On the other hand, κ_{Ty} shows a slightly nonlinear dependence on temperature, an effect likely due to variation of composite layer's CTE in the direction perpendicular to the fibers. These measured thermal curvatures serve as the loading inputs used to generate modeling results for the following sections.

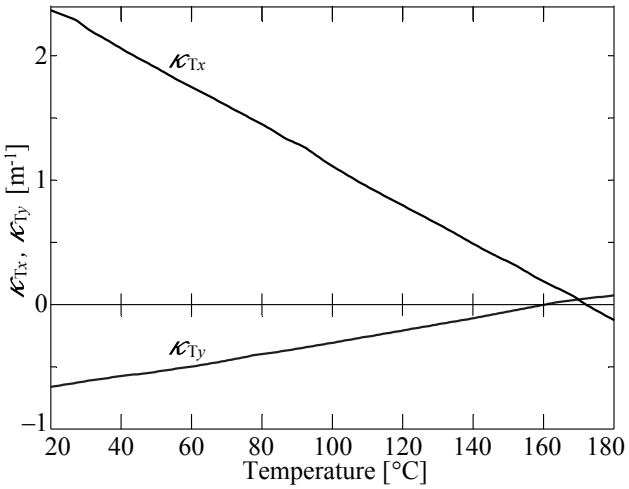

Figure 6. Experimentally measured thermal curvatures of the strip specimens described in Table 2.

V.B. Model Predictions Regarding the Influence of Initial Curvature

A stability map is given in Fig. 7 for the laminate specified in Table 2.[f] The results are plotted for various initial curvatures to demonstrate its effects upon the laminate's response to thermal loading. The bistable regions for each initial curvature are simply copies of each-

[f]The stability map presented in Fig. 7 is similar to that in Fig. 2, however the bistable regions are now specified in terms of thermal curvatures rather than thermally induced internal moments in keeping with our experimental approach. This effectively amounts to rescaling each axis proportional to the laminate's respective bending stiffnesses. Thus, the shapes of the bistable regions in Fig. 7 are distorted from their appearance in Fig. 2 due to the laminate's flexural anisotropy.

other shifted along the y-axis by a value opposite to their corresponding initial curvatures. This interesting feature is only observed when the initial shape is a developable surface. Elaborating upon that statement, for non-developable initial shapes , initial curvature enters Eq. (14) both via the midplane stretching vector $\boldsymbol{\epsilon}^0$ and the curvature change vector $\Delta\boldsymbol{\kappa}$. However, $\boldsymbol{\epsilon}^0$ only contains initial curvature terms in the form of $\hat{a}\hat{b}-\frac{\hat{c}^2}{4}$ (see Eq. (7)). This form represents the Gaussian curvature of the initial shape, and thus for the case of developable initial shapes, these terms collectively vanish. Thus, the only remaining avenue for initial curvature to enter Eq. (14) is via $\Delta\boldsymbol{\kappa}$. With the the aid of Eq. (3), the curvature terms of Eq. (14) can be expanded as $\Delta\kappa_i - \kappa_{\mathrm{T}i} = \kappa_i - (\hat{\kappa}_i + \kappa_{\mathrm{T}i})$. This form makes it apparent that initial curvature appears in the same term as thermal curvature, and thus we can see that the effect of initial curvature is equivalent to the respective thermal curvature, so long as the initial curvature is developable. It also follows that any potential energy minimum attained with zero initial curvature can be duplicated exactly for cylindrical initial curvature by offsetting the values of each thermal curvature term by the opposite of the respective initial curvature values. Thus, we see in Fig. 7 that the bistability regions are shifted along a thermal curvature axis by an amount opposite to the corresponding initial curvature.

The experimentally measured thermal curvatures are plotted as the dashed line in Fig. 7. This thermal curvature path starts at a point near the origin, which corresponds to the laminate's cure temperature. The fact that this path does not start coincident with the origin indicates the presence of non-thermoelastic strains at cure temperature. Proceeding to the right along the thermal curvature path, the magnitude of $\kappa_{\mathrm{T}x}$ grows much faster than the magnitude of $\kappa_{\mathrm{T}y}$, by a factor of approximately 3.5. This trend is due to the higher CTE mismatch of the metallic and composite layers in the fiber 0° direction relative to the 90° direction. Upon further cooling, the thermal curvature path intersects the bistability regions for $\hat{\kappa}_y = -2.0\,\mathrm{m}^{-1}$, $-2.5\,\mathrm{m}^{-1}$, and $-3.0\,\mathrm{m}^{-1}$. Snap-through upon cooling is predicted at points b, e, and f, respective to each initial curvature. The temperatures and shell curvatures corresponding to these points are indicated by the matching letters in Fig. 8. Upon re-heating, snap-through is predicted at points a, c, or d, respective to each initial curvature. Laminates of the presently investigated stacking sequence are not predicted to exhibit bistable or snap-through properties when they possess initial curvatures of greater than approximately $-1.63\,\mathrm{m}^{-1}$, evidenced by the failure of those regions to intersect the thermal curvature path. However, it can still be seen from Fig. 8 that even when this behavior is not predicted, the resulting curvature-temperature relationship may still be highly nonlinear, especially for cases of initial curvature which nearly trigger bistable behavior, e.g. $\hat{\kappa}_y = -1.5\,\mathrm{m}^{-1}$. Increasing the magnitude of initial curvature increases the magnitude of ΔT required to trigger snap-through, while also widening the temperature range over which bistability exists. This behavior can be visualized in Fig. 7, where shifting a given region upwards results in a

rightwards shift of the points where the thermal curvature path intersects this region.

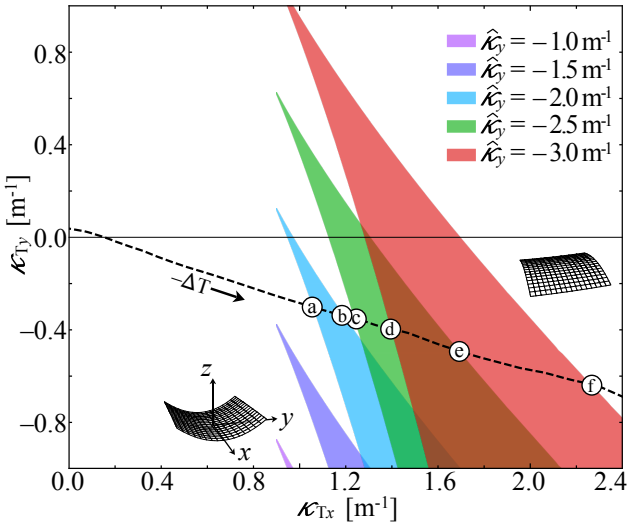

Figure 7. Stability map showing combinations of thermal curvatures $\kappa_{\mathrm{T}x}$ and $\kappa_{\mathrm{T}y}$, and initial curvatures $\hat{\kappa}_y$ which yield bistable behavior, denoted by colored regions. The dashed line represents the path of thermal curvatures experimentally measured in Subsection IV.B, while the circular markers denote snap-through points passed upon heating or cooling for various initial curvatures. The temperature and curvatures at snap-through initiation are indicated by the corresponding letters in Fig. 8. The shell illustrations adjacent to the regions represent the two stable shapes attained within each region, as well as the monostable shapes which exist outside each respective region boundary.

V.C. Model Predictions of the Laminate's Response to Thermal Loads

Results for the fiber-metal hybrid laminated shell and beam specimens described in Table 2 are given in Fig. 9. The thermal curvature changes measured in the 0° and 90° strip specimens are superimposed upon the initial curvatures of the plate in their respective directions to yield the plate's *natural curvatures* $\kappa_{\mathrm{N}i}$, defined explicitly as $\kappa_{\mathrm{N}i} = \kappa_{\mathrm{T}i} + \hat{\kappa}_i$. Thus, the dashed lines indicate the curvature that the initially curved shell would achieve if not for the buildup of membrane stress on account of Gaussian curvature growth. As our shell has zero Gaussian curvature in its initial state, and because its thinness makes it relatively stiff in membrane stretching relative to bending, it tends to conserve Gaussian curvature as thermal loads are applied. That is to say that in this case, it always tends to have at least one principal curvature be zero, or at least nearly zero. This supposition is verified by both our analytical and experimental data, which show that regardless of temperature, at least one of the shell curvatures κ_x or κ_y is nearly zero.

As the shell is cooled from its cure temperature to 100°C, the analytical and experimentally predicted κ_x quickly diverges from $\kappa_{\mathrm{N}x}$. This response is due to the role of initial curvature, which stiffens the laminate against the internal bending moments via development of membrane strain, as the laminate had to develop nonzero Gaussian curvature in order to incur a change in κ_x. Meanwhile, κ_y is also nearly constant while cooling to 100°C, despite the increasing magnitude of $\kappa_{\mathrm{N}y}$. The apparent inertness to thermal loading is a

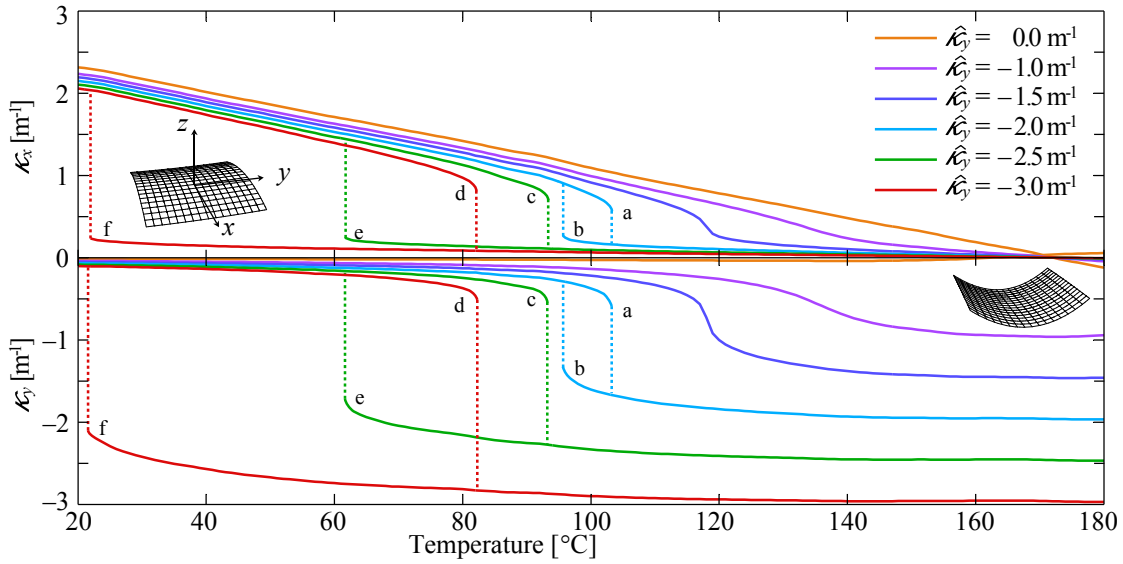

Figure 8. Analytical results showing predicted effect of initial curvature upon hybrid laminate response to thermal loading. Vertical dotted lines represent snap-through paths. The cure temperature is 180°C, and thus the magnitude of thermal loading increases for decreasing temperatures.

result of competition between the thermally induced moments along the y-direction, and Brazier loads induced by much greater thermal moments along the x-direction . Effectively, the shell's tendency to respond to changes in $\kappa_{\mathrm{T}y}$ with additional curvature magnitude is approximately balanced by the curvature reduction induced by the shell's tendency to collapse towards its neutral axis on account of the much greater bending moment along the x-direction. When cooled further, the Brazier loads eventually out-compete the moments induced by $\kappa_{\mathrm{T}y}$, and the result is a snap-through change of shape to a cylinder with principal curvature oriented along the x-direction. The analytical model predicted this event to take place upon cool-down through 61°C.

The motivation for a transition to major curvature in the x-direction can also be viewed from an energy minimization perspective. By observing Eq. (14), we can see that potential energy scales linearly with the laminate stiffness terms, but quadratically to the mismatch between the terms of the $\Delta\boldsymbol{\kappa}$ and $\boldsymbol{\kappa}_{\mathrm{T}}$ vectors.[g] Thus, we deduce that stable shapes have this curvature mismatch preferentially minimized along the stiffest direction. In other words, we expect that after some degree of thermal loading, the laminate develops curvature in similar orientation and magnitude to the thermal curvature component of greatest magnitude, especially if this component corresponds to the same direction for which flexural stiffness is maximized. This basic explanation neglects the membrane strain terms, and unsurprisingly, we see that it breaks down in the temperature range where the shell's initial curvature restricts curvature development in the orthogonal direction, on account of the significant role

[g]This relationship is analogous to the equation for strain energy density stored in a body under uniaxial load, $\Pi = \frac{1}{2}E\epsilon^2$.

that membrane effects play under these conditions.

Below the cooling snap-through temperature, κ_y is almost entirely suppressed by dominate κ_x. With further cooling, κ_x continues to grow at an approximately linear rate. Upon heating from room temperature, the shell curvatures initially retrace their cooling paths, however now their heating snap-through temperature is markedly offset from the cooling snap-through temperature. Both experiment and analysis show the heating snap-through to take place at 93°C, at which point the laminate reverts back to its initial shape. Both κ_x and κ_y remain approximately constant throughout the remaining heating interval.

V.D. Experimental Results

The experimental results show two separate types of hysteretic behavior, the first being due to geometrically nonlinear effects, while the second is likely due to material nonlinearity. With regards to the first, because the heating and cooling snap-through temperatures are separated by a gap of 22°C, the laminate displays clear *deadband hysteresis.* This behavior is similar to that displayed by prebuckled bimorph beams,[13] such as those used in thermostats and circuit breakers. Effectively, our laminate achieves this sort of behavior by buckling under its own thermal stresses, as opposed to relying upon constraining boundary conditions as is the case for prebuckled beams. This behavior suggests that snap-through laminates may be particularly useful for passive thermal control applications, where a degree of deadband hysteresis is desirable to avoid chatter behavior. From a design standpoint, the width of the temperature deadband may be tailored by adjusting the initial curvature, as demonstrated by Fig. 7. The deadband range scales with the length of the intersection between the dashed line and a given bistable region in that figure. Changes to the laminate's constitutive properties and planform shape will also impact the deadband range.

The second type of hysteresis occurs at higher temperatures, and is responsible for the mismatch between the heating and cooling values of κ_y measured above 93°C. Bearing in mind that the experiment featured a heating ramp followed by cooling, we observe κ_y to be slightly higher upon cooling than heating. Some clues to this behavior are offered if we recall that the y-direction internal thermal moment (and its associated thermal curvature) are driven by CTE mismatch between the aluminum and 90° composite layers. Given that the 90°material properties are matrix-dominated, we can hypothesize that viscoelastic stress-relaxation of the polymer matrix, or potentially drying of residual moisture content within the matrix may be at play. Our focus on the matrix properties is supported by the fact that there is no similar hysteresis observed in κ_x, whose behavior is expected to be a result of fiber-dominated properties instead.

Between the heating and cooling snap-through temperatures, the laminate is bistable, and may be snapped from one cylindrical orientation to another by application of external

forces.

V.E. Comparison of model predictions with experimental results

The analytical model showed excellent correlation with experiment below the cooling snap-through temperature. Above the heating snap-through temperature, the model failed to predict the aforementioned material hysteresis, resulting in error of κ_y prediction of up to 24%. The model had mixed results predicting the snap-through temperatures of the laminate, with the cooling snap-through prediction diverging from experiment by 9°C, although the heating snap-through was predicted accurately. It is likely that the seemingly accurate prediction of the heating snap-through temperature is at least partly due to coincidence, and that what we are actually observing is a lucky cancellation of errors in both the prediction of the range and midpoint temperature of the bistability temperature range. In other words the model's deadband hysteresis loop is not only too wide, but also offset slightly in terms of temperature from the experimental results, such that the two heating snap-through temperatures happen to be coincident. The model's overprediction of the deadband range indicates that it is overestimating the thermal loads required for snap-through. This observation is in agreement with the work of Pirrera et al.[42] and Lamacchia et al.,[43] who show that the constant curvature shape functions used in this work overconstrain the laminate's kinematics during snap-through transitions, compared to models with more degrees of freedom.

Should such a class of laminate be implemented as an actuation device, the designer will most likely be concerned primarily with κ_x rather than κ_y on account of the fact that both stiffness and curvature generation capability of the laminate are maximized along the x-direction. In this case, the model's predictions of κ_x are generally quite accurate.

VI. Conclusion

The use of composite materials and exploitation of geometric nonlinearity enables creation of bimorph structures with highly nonlinear responses to temperature change. In the case of thermal bimorphs, where internal moments are proportional to temperature change, initial curvature is necessary to yield thermally driven snap-through behavior in free-standing shells. The snap-through process is characterized by a transition from one stable shape to another, and occurs instantaneously when a bistable shell in one shape reverts to a state of monostability characterized by the alternate stable shape. This condition cannot be met when the internal moments are equal and opposite sign. Instead, the internal moments must be equal and same sign, or possess a high degree of orthotropy in which the major internal moment is oriented both perpendicular and opposite sign to the initial curvature.

In order to model these responses, an extended energy-based multistability model is pro-

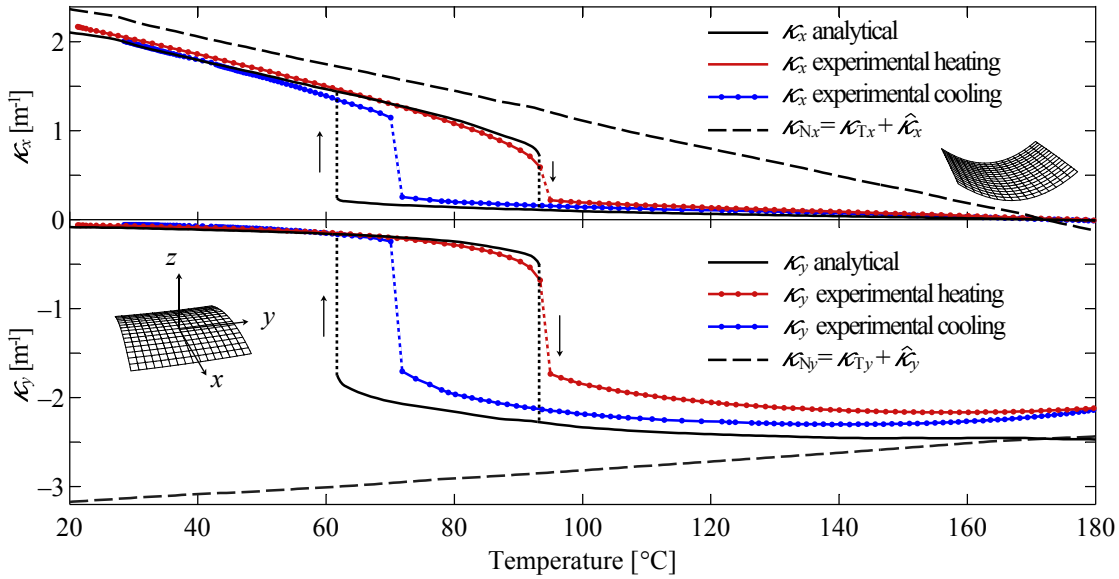

Figure 9. Experimental results of shell curvatures compared to model predictions for the laminate described in Table 2. Vertical dotted lines represent snap-through paths, which proceed along the direction indicated by arrows.

posed in which loads are input in terms of experimentally measured thermal curvatures. This strategy bypasses the need to measure the thermal expansion coefficients of each constituent material, and automatically accounts for non-thermoelastic strains. This model has been applied to the prediction of a nonlinear bimorph's curvature response to temperature change. Experimental observation of an initially curved shell's curvature-temperature relationship matched well with analytical predictions at lower temperatures, however, discrepancy was observed at higher temperatures, likely on account of material behavior that departed from our linear elastic assumptions. The shell displayed snap-through behavior when heated and cooled, and displayed deadband hysteretic behavior when cycled above and below its snap-through temperatures.

The use of nonlinear bimorphs opens the possibility of temperature-actuated aerodynamic control surfaces on a variety of scales. Particular appeal may be found within gas turbine engines, whereby component geometry and cooling flow may be optimized for across a variety of engine operating states, using the gas-path temperature changes inherent in each operating state as the driving control inputs. Nonlinear bimorphs may also be useful on smaller scales, including micro-fluidic controls and nanoscale electrical switches.[44,45]

Acknowledgments

The authors would like to thank the reviewers for their many helpful and insightful comments. This work was sponsored by the European Office of Air Force Research and Development, Air Force Office of Scientific Research, USAF, under grant number FA9550-14-1-0063. The U.S. Government is authorized to reproduce and distribute reprints for governmental purpose

notwithstanding any copyright notation thereon. The views and conclusions contained herein are those of the authors and should not be interpreted as necessarily representing the official policies or endorsements, either expressed or implied, of the Air Force Office of Scientific Research or the U.S. Government. This work was also supported by the Engineering and Physical Sciences Research Council through the EPSRC Centre for Doctoral Training in Advanced Composites for Innovation and Science, grant number EP/G036772/1.

References

[1]Chang, M. H. and Mancuso, R., "A compilation of design and performance characteristics for thermal louver systems," *19th Thermophysics Conference*, American Institute of Aeronautics and Astronautics, June 1984.

[2]Calkins, F. T., Mabe, J. H., and Butler, G. W., "Boeing's variable geometry chevron: morphing aerospace structures for jet noise reduction," *Proceedings of SPIE*, Vol. 6171, No. 1, March 2006.

[3]Lattime, S. B. and Steinetz, B. M., "High-pressure-turbine clearance control systems: current practices and future directions," *Journal of Propulsion and Power*, Vol. 20, No. 2, 2004, pp. 302–311.

[4]Brampton, C. J., Bowen, C. R., Buschhorn, S. T., Lee, J., Pickering, S. G., Wardle, B. L., and Kim, H. A., "Actuation of Bistable Laminates by Conductive Polymer Nanocomposites for use in Thermal-Mechanical Aerosurface De-icing Systems," *55th AIAA/ASMe/ASCE/AHS/SC Structures, Structural Dynamics, and Materials Conference*, American Institute of Aeronautics and Astronautics, Jan. 2015.

[5]Asanuma, H., Hakoda, G., and Mochizuki, T., "Fabrication of Nickel Based Active Composites," *JSME International Journal Series A Solid Mechanics and Material Engineering*, Vol. 46, No. 3, 2003, pp. 473–477.

[6]Eckstein, E., Weaver, Paul M., A., and Halbig, M. C., "Thermally-Driven Morphing with High Temperature Composites," *57th AIAA/ASCE/AHS/ASC Structures, Structural Dynamics, and Materials Conference*, American Institute of Aeronautics and Astronautics, Jan. 2016.

[7]Mercer, C. R., Haller, W. J., and Tong, M. T., "Adaptive Engine Technologies for Aviation CO2 Emissions Reduction," Tech. Rep. NASA/TM-2006-214392, Aug. 2006.

[8]Wei, Z. G., Sandstrorom, R., and Miyazaki, S., "Shape-memory materials and hybrid composites for smart systems: Part I Shape-memory materials," *Journal of Materials Science*, Vol. 33, No. 15, Aug. 1998, pp. 3743–3762.

[9]Priebe, J., "The utilization of High Output Paraffin actuators in aerospace applications," *31st Joint Propulsion Conference and Exhibit*, American Institute of Aeronautics and Astronautics, July 1995.

[10]Ho, C. Y. and Taylor, R. E., *Thermal Expansion of Solids*, ASM International, 1998.

[11]Mansfield, E. H., "Bending, Buckling and Curling of a Heated Elliptical Plate," *Proceedings of the Royal Society of London. Series A. Mathematical and Physical Sciences*, Vol. 288, No. 1414, Nov. 1965, pp. 396–417.

[12]Gigliotti, M., Wisnom, M. R., and Potter, K. D., "Loss of bifurcation and multiple shapes of thin [0/90] unsymmetric composite plates subject to thermal stress," *Composites Science and Technology*, Vol. 64, No. 1, Jan. 2004, pp. 109–128.

[13]Timoshenko, S., "Analysis of bi-metal thermostats," *J. Opt. Soc. Am*, Vol. 11, No. 3, 1925.

[14]Mansfield, E. H., "Bending, Buckling and Curling of a Heated Thin Plate," *Proceedings of the Royal Society of London. Series A. Mathematical and Physical Sciences*, Vol. 268, No. 1334, July 1962, pp. 316–327.

[15]Seffen, K. A. and McMahon, R. A., "Heating of a uniform wafer disk," *International Journal of Mechanical Sciences*, Vol. 49, No. 2, Feb. 2007, pp. 230–238.

[16]Hyer, M. W. and Bhavani, P. C., "Suppression of anticlastic curvature in isotropic and composite plates," *International Journal of Solids and Structures*, Vol. 20, No. 6, 1984, pp. 553–570.

[17]Brazier, L. G., "On the flexure of thin cylindrical shells and other thin sections," *Proceedings of the Royal Society of London. Series A*, Vol. 116, No. 773, 1927, pp. 104–114.

[18]Ren, L., Parvizi-Majidi, A., and Li, Z., "Cured Shape of Cross-Ply Composite Thin Shells," *Journal of Composite Materials*, Vol. 37, No. 20, Oct. 2003, pp. 1801–1820.

[19]Pellegrino, S., "Large retractable appendages in spacecraft," *Journal of Spacecraft and Rockets*, Vol. 32, No. 6, 1995, pp. 1006–1014.

[20]Eckstein, E., Pirrera, A., and Weaver, P., "Multi-mode morphing using initially curved composite plates," *Composite Structures*, Vol. 109, March 2014, pp. 240–245.

[21]Fernandes, A., Maurini, C., and Vidoli, S., "Multiparameter actuation for shape control of bistable composite plates," *International Journal of Solids and Structures*, Vol. 47, No. 10, May 2010, pp. 1449–1458.

[22]Hyer, M., "Calculations of the Room-Temperature Shapes of Unsymmetric Laminates," *J Composite Materials*, Vol. 15, Jan. 1981, pp. 296.

[23]Asanuma, H., Haga, O., and Imori, M., "Development of High Performance CFRP/Metal Active Laminates," *JSME International Journal Series A*, Vol. 49, No. 1, 2006, pp. 32–37.

[24]Halpin, J. C. and Pagano, N. J., "Consequences of environmentally induced dilatation in solids," Tech. Rep. AD-701-725, United States Air Force Research Laboratory, Dec. 1969.

[25]Guest, S. and Pellegrino, S., "Analytical models for bistable cylindrical shells," *Proceedings of the Royal Society A: Mathematical, Physical and Engineering Science*, Vol. 462, No. 2067, March 2006, pp. 839 –854.

[26]Pirrera, A., Avitabile, D., and Weaver, P., "On the thermally induced bistability of composite cylindrical shells for morphing structures," *International Journal of Solids and Structures*, Vol. 49, No. 5, March 2012, pp. 685–700.

[27]Seffen, K. A., "Morphing bistable orthotropic elliptical shallow shells," *Proceedings of the Royal Society of London A: Mathematical, Physical and Engineering Sciences*, Vol. 463, No. 2077, Jan. 2007, pp. 67–83.

[28]Dano, M.-L. and Hyer, M. W., "Thermally-induced deformation behavior of unsymmetric laminates," *International Journal of Solids and Structures*, Vol. 35, No. 17, June 1998, pp. 2101–2120.

[29]Daynes, S. and Weaver, P. M., "Analysis of unsymmetric CFRP-metal hybrid laminates for use in adaptive structures," *Composites Part A: Applied Science and Manufacturing*, Vol. 41, No. 11, Nov. 2010, pp. 1712–1718.

[30]Radford, D. W. and Rennick, T. S., "Separating Sources of Manufacturing Distortion in Laminated Composites," *Journal of Reinforced Plastics and Composites*, Vol. 19, No. 8, May 2000, pp. 621–641.

[31]Seffen, K. A. and Maurini, C., "Growth and shape control of disks by bending and extension," *Journal of the Mechanics and Physics of Solids*, Vol. 61, No. 1, Jan. 2013, pp. 190–204.

[32]Vidoli, S. and Maurini, C., "Tristability of thin orthotropic shells with uniform initial curvature," *Proceedings of the Royal Society of London A: Mathematical, Physical and Engineering Sciences*, Vol. 464, No. 2099, Nov. 2008, pp. 2949–2966.

[33]Mansfield, E. H., *The Bending and Stretching of Plates*, Cambridge University Press, 2nd ed., 1989.

[34]Mattioni, F., Weaver, P. M., and Friswell, M. I., "Multistable composite plates with piecewise variation of lay-up in the planform," *International Journal of Solids and Structures*, Vol. 46, No. 1, Jan. 2009, pp. 151–164.

[35]Brunetti, M., Vincenti, A., and Vidoli, S., "A class of morphing shell structures satisfying clamped boundary conditions," *International Journal of Solids and Structures*, 2016.

[36]Calladine, C. R., *Theory of Shell Structures*, Cambridge University Press, Cambridge, 1983.

[37]Reddy, J. N., *Mechanics of Laminated Composite Plates and Shells: Theory and Analysis, Second Edition*, CRC Press, Boca Raton, 2nd ed., Nov. 2003.

[38]Collier, C. S., "Stiffness, thermal expansion, and thermal bending formulation of stiffened, fiber-reinforced composite panels," *AIAAASCE/AHS/ASC Structures, Structural Dynamics, and Materials Conference, 34th and AIAA/ASME Adaptive Structures Forum*, April 1993.

[39]Betts, D. N., Kim, H. A., Bowen, C. R., and Inman, D. J., "Optimal configurations of bistable piezo-composites for energy harvesting," *Applied Physics Letters*, Vol. 100, No. 11, March 2012.

[40]Peraza Hernandez, E. A., Kiefer, B., Hartl, D. J., Menzel, A., and Lagoudas, D. C., "Analytical investigation of structurally stable configurations in shape memory alloy-actuated plates," *International Journal of Solids and Structures*, Vol. 69-70, Sept. 2015, pp. 442–458.

[41]*ESDU Metallic Materials Data Handbook, Section 6: Aluminium Alloys*, Supplement 47, IHS ESDU, July 2012.

[42]Pirrera, A., Avitabile, D., and Weaver, P., "Bistable plates for morphing structures: A refined analytical approach with high-order polynomials," *International Journal of Solids and Structures*, Vol. 47, No. 25-26, Dec. 2010, pp. 3412–3425.

[43]Lamacchia, E., Pirrera, A., Chenchiah, I. V., and Weaver, P. M., "Morphing shell structures: A generalised modelling approach," *Composite Structures*, Vol. 131, Nov. 2015, pp. 1017–1027.

[44]Schaeffler, N., Hepner, T., Jones, G., and Kegerise, M., "Overview of Active Flow Control Actuator Development at NASA Langley Research Center," *1st Flow Control Conference*, American Institute of Aeronautics and Astronautics, June 2002.

[45]Pott, V., Cohen, H., Nathanael, R., Jeon, J., Alon, E., and Liu, T., "Mechanical Computing Redux: Relays for Integrated Circuit Applications," *Proceedings of the IEEE*, Vol. 98, No. 12, Dec. 2010, pp. 2076–2094.